Proceedings of EuCoMeS, the first
European Conference on Mechanism Science
Obergurgl (Austria), February 21–26 2006
Manfred Husty and Hans-Peter Schröcker, editors

Error workspace analysis of planar mechanisms

Adolf Hofmeister* Walter Sextro* Otto Röschel†

In this paper the unconstrained motion (Error workspace) of some planar systems with joint clearance is analyzed. For the analysis, the joints are assumed to be revolute or translational. We also assume that all joint clearances are known. The kinematic image space is used to provide a geometric environment for the analysis of Error workspace. In this paper the Error workspace of a four-bar linkage, of a slider-crank mechanism and of two multiple-loop mechanisms are studied. Furthermore, mechanisms which have folding positions due to joint clearance are studied, too.

Introduction

Joint clearances of mechanisms are the consequences of manufacturing errors or of mechanical wear. Mechanisms of single degree of freedom have constrained motion if one input is applied. If joint clearance is significantly large, the motion of the linkage becomes unconstrained. Many investigations have been devoted to the study of joint clearance. Hörsken (2003) used the Monte-Carlo method for tolerance analysis in multibody systems and computer aided design. Wittwer et al. (2004) used the direct linearization method applied to position error in kinematic linkage. Tsai and Lai (2004) demonstrated a method to analyze the transmission performance of linkages that have joint clearance. Voglewede and Uphoff (2004) described in detail the clearances of revolute joints and translational joints and study the unconstrained motion of parallel manipulators near singular configurations. Pernkopf and Husty (2005) presented an analysis of the reachable workspace of a spatial Stewart-Gough-Platform with planar base and platform (SGPP) and demonstrated by means of the results of this workspace analysis, the influence of joint clearance and manufacturing erros. Wohlhart (1999) studied the effect of a single small translatorial backlash in one of the linear actuators of a planar and of a spatial (Stewart-Gough) platform, in singular positions at various degrees of shakiness. Schröcker and Wallner (2005) and Wallner et al. (2005) treated the problems of tolerances in general cases: Either they used balls of affine transformations or they estimated tolerance zones. With help of approximations they gave bounds for the error of estimated tolerances. Frick (2004) used

*Institute of Mechanics, Graz, University of Technology, a.hofmeister@tugraz.at, sextro@TUGraz.at
†Institute of Geometry, Graz, University of Technology, roeschel@TUGraz.at

the the kinematic mapping and an ANSI-C program to study and describe "unstable" four-bar motion and "unstable" RPR-platform for increasing tolerance values.

If we restrict to planar Euclidean mechanisms we are able to give exact descriptions of Error workspaces (EWS) for four-bar and slider-crank mechanism. We will use the kinematic mapping in order to gain descriptions of the Orientation Error workspace (Ori-EWS) (= all orientations which can be reached in at least one position) and of the Position Error workspace (Pos-EWS) (= all positions which can be reached in at least one orientation). Each error (clearance) at a linkage gives higher order mobility, which is displayed in the kinematic image space. Our goal is to optimize the design of mechanisms by taking into account manufacturing errors or mechanical wear.

The special example of a planar four-bar mechanism is worked out in detail in section 3.1. Section 4 is devoted to case studies for composed four-bar mechanisms, in section 5 we extend our considerations to slider-crank mechanisms.

1 Mapping of Plane Kinematics

A direct displacement $\mathcal{D}$ of the Euclidean plane transforms a frame Σ with respect to a fixed frame Σ_0. It is determined by three independent parameters (a, b, φ) – a and b determine the translational part, φ fixes the angle of rotation. Points $P(x, y)$ of Σ and $P_0(X, Y)$ of Σ_0 are given by Cartesian and corresponding homogenous coordinates $(\bar{x} : \bar{y} : \bar{z}) = (x : y : 1)$ and $(\bar{X} : \bar{Y} : \bar{Z}) = (X : Y : 1)$, respectively. Then we have $\mathcal{D} : \Sigma \to \Sigma_0$ with

$$\begin{pmatrix} \bar{X} \\ \bar{Y} \\ \bar{Z} \end{pmatrix} = \begin{pmatrix} \cos(\varphi) & -\sin(\varphi) & a \\ \sin(\varphi) & \cos(\varphi) & b \\ 0 & 0 & 1 \end{pmatrix} \begin{pmatrix} \bar{x} \\ \bar{y} \\ \bar{z} \end{pmatrix}. \tag{1}$$

The kinematic mapping $\varkappa : SE(2) \to \mathbb{P}^3$ maps the direct displacement $\mathcal{D}(a, b, \varphi)$ to a point $\varkappa(\mathcal{D})$ of a real projective 3-space $\mathbb{P}^3$, see Blaschke (1960) and Bottema and Roth (1990). Points of $\mathbb{P}^3$ are given in homogenous coordinates $(X_1 : X_2 : X_3 : X_4)$, where $\varkappa(\mathcal{D})$ is defined as

$$(X_1 : X_2 : X_3 : X_4) = (a\sin(\varphi/2) - b\cos(\varphi/2) : a\cos(\varphi/2) + b\sin(\varphi/2) : 2\sin(\varphi/2) : 2\cos(\varphi/2)) \tag{2}$$

The points of the straight line $u(X_3 = X_4 = 0)$ are no images of displacements. Therefore the image space of $\varkappa$ is restricted to the part $\mathbb{Q}^3 := \mathbb{P}^3 - \{P \in u\}$. The kinematic mapping $\varkappa$ is a bijective mapping of the direct Euclidean displacements $SE(2)$ to the points of $\mathbb{Q}^3$.

Changes of the Cartesian frames in Σ and Σ_0 change the image points $\varkappa(D)$ – this way the image space gets the structure of a quasielliptic space with the real absolute line u – see Blaschke (1960). The quasielliptic differential geometry is developed by Stachel (1970).

The quasielliptic planes through u are called "horizontal" planes. The metric induced in these planes is a Euclidean one (with u at infinity). Therefore it is quite natural to use an auxiliary Euclidean 3-space to visualize the properties of $\mathbb{Q}^3$. In these cases we will normalize the coordinates by $X_4 = 1$ (if possible).

Now we start with a point $P \in \mathbb{Q}^3$: If we eliminate a, b, φ from (1) and (2) we are able to express the action of $\varkappa^{-1}(P)$ by

$$\begin{pmatrix} \bar{X} \\ \bar{Y} \\ \bar{Z} \end{pmatrix} = \begin{pmatrix} (X_4^2 - X_3^2) & -2X_3X_4 & 2(X_1X_3 + X_2X_4) \\ 2X_3X_4 & (X_4^2 - X_3^2) & 2(X_2X_3 - X_1X_4) \\ 0 & 0 & (X_4^2 + X_3^2) \end{pmatrix} \begin{pmatrix} \bar{x} \\ \bar{y} \\ \bar{z} \end{pmatrix} \tag{3}$$

$\mathcal{D} = \kappa^{-1}(P)$ maps the point $E(\bar{x} : \bar{y} : \bar{z})$ of Σ into $E_0(\bar{X} : \bar{Y} : \bar{Z})$ of Σ_0.

Remark 1. All points $P(X_1 : X_2 : X_3 : X_4)$ which belong to fixed points $E(\bar{x} : \bar{y} : \bar{z})$ and $E_0(\bar{X} : \bar{Y} : \bar{Z})$ are situated on the straight line through the two points $P_1(\bar{y}\bar{Z} - \bar{z}\bar{Y} : \bar{z}\bar{X} - \bar{x}\bar{Z} : 0 : 2\bar{z}\bar{Z})$ and $P_2(\bar{z}\bar{X} + \bar{x}\bar{Z} : \bar{z}\bar{Y} + \bar{y}\bar{Z} : 2\bar{z}\bar{Z} : 0)$. If we vary E_0, these lines form an elliptic line congruence LC_E, which depend on the input data point $E \in \Sigma$. So E_0 can be gained directly as the image of the original point P under a (quadratic) projection $\gamma_E : \mathbb{Q}^3 \to \Sigma_0$. For more detail see Bereis (1964).

1.1 Circular and linear constraints

Bottema and Roth (1990) and Husty (1996) have shown the kinematic image of the motion of a fixed point $E(x, y)$ in Σ that is constrained to move on a fixed circle k_0 in Σ_0 with radius r centered on the Cartesian coordinates (M_X, M_Y) and having the equation

$$k_0 \ldots (X - M_X)^2 + (Y - M_Y)^2 - r^2 = 0 \tag{4}$$

is an hyperboloid $\mathcal{H}_M$ of one sheet with equation

$$\left(X_1 - \frac{1}{2}(-M_Y + y + X_3(x + M_X))\right)^2 + \left(X_2 - \frac{1}{2}(M_X - x + X_3(y + M_Y))\right)^2 = \frac{1}{4}r^2(1 + X_3^2). \tag{5}$$

In quasielliptic geometry this is a quadric of revolution. Its axis a_M is the reciprocal polar of the line u. It has the linear parametric representation

$$\begin{bmatrix} X_1 \\ X_2 \\ X_3 \end{bmatrix} = \frac{1}{2}\begin{bmatrix} -M_Y + y \\ M_X - x \\ 0 \end{bmatrix} + \frac{t}{2}\begin{bmatrix} M_X + x \\ M_Y + y \\ 2 \end{bmatrix} \qquad \text{by setting } X_3 = t. \tag{6}$$

Remark 2. The hyperboloid axis a_M does not depend on the radius r of the circle k_0. The axis a_M itself belongs to $r = 0$ – the point $E(x, y)$ in Σ remains fixed at (M_X, M_Y) in Σ_0.

If the fixed point $E(x, y)$ in Σ moves on a line l_0 (fixed in Σ_0) with the equation

$$l_0 \ldots AX + BY + C = 0, \tag{7}$$

the kinematic images of the corresponding displacements are points of an hyperboloid of one sheet again. It contains the absolute line u – in our auxiliary Euclidean description it is an hyperbolic paraboloid HP:

$$\begin{aligned} &-A{X_3}^2 x + Ax - 2\,AX_3\,y + 2\,AX_3\,X_1 + 2\,AX_2 - 2\,BX_1 + By - By{X_3}^2 + \\ &\quad 2\,BX_3\,x + 2\,BX_3\,X_2 + C + C{X_3}^2 = 0. \end{aligned} \tag{8}$$

2 Unconstrained Joint Motion

This section describes the Positions Error workspace (all possible positions) of joints taking clearances into account. We assume that the joint clearance is known. In this paper we look at two types of joints: the revolute joint and the translational joint. The key point is to construct a virtual mechanism with which the Pos-EWS is easier to describe.

2.1 Joint clearance of a revolute joint

Fig. (1a) shows a revolute joint with joint clearance. Assuming a perfect circular hole and pin (radii r_0, r_1), the center L_1 of the pin is allowed to move in a circular region of radius $\varepsilon_1 = r_0 - r_1$. This revolute joint is equivalent to the virtual link Fig. (1b). The radius ε_1 of the virtual link describes the possible motion of pin center L_1. So ε_1 is the radius of joint clearance of the link L_1.

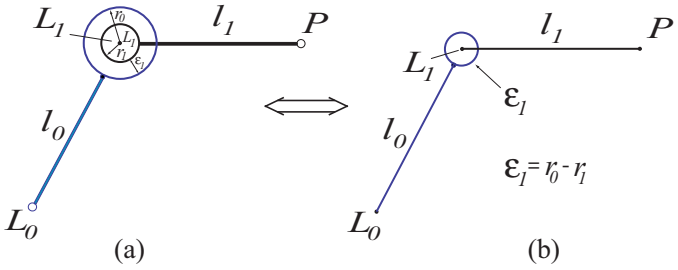

Figure 1: Revolute joint with clearance

2.2 Unconstrained motion of a chain of revolute joints

Also the Pos-EWS of a chain of revolute joints with clearance can be described. Fig. (2) shows three virtual revolute joints connected in series with the first joint L_0 (is fixed). Let ε_1 and ε_2 be the clearance of the joints L_1 and L_2 and l_0 and l_1 the length of the legs. In Fig. (2) we can see possible positions of the point L_2, which belongs to a ring $\mathbf{B}(L_2)$ centered at L_1. It has the following range for its radius $r : (l_1 - (\varepsilon_1 + \varepsilon_2)) \leq r \leq (l_1 + (\varepsilon_1 + \varepsilon_2))$, if $l_1 \geq (\varepsilon_1 + \varepsilon_2)$.

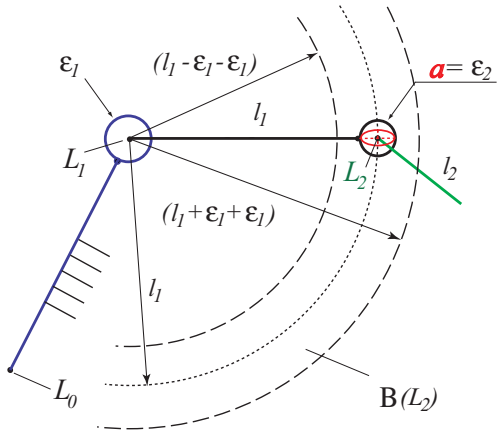

Figure 2: Pos-Error workspace of L_2

Remark 3. All possible locations of the point L_2 describe the same ring $\mathbf{B}(L_2)$, if the virtual hole in link L_2 is not a circle but, for example, an ellipse like the red curve in Fig. (2) with semimajor axis $a = \varepsilon_1$. For the Pos-EWS $\mathbf{B}(L_2)$ only the maximum and the minimum distance from pin center L_1 to the connected link hole of L_2 are important.

The ring $\mathbf{B}(L_2)$ can also be created by a virtual prismatic joint with the limits of the length: $l : (l_1 - (\varepsilon_1 + \varepsilon_2)) \leq l \leq (l_1 + (\varepsilon_1 + \varepsilon_2))$. In this way you can take as many revolute joints as you like and connect them in series and the Pos-EWS of the centers L_i are annular regions or circular disks.

2.3 Joint clearance of a translational joint

Fig. (3a) shows a translational joint with joint clearance. Assuming a perfect sliding block and a slide the translational joint is equivalent to the virtual joint, see Fig. (3b). All possible locations of L_1 belong to a strip; the thickness of the strip is $\delta_1 = h_0 - h_1$ (clearance between sliding block and slide).

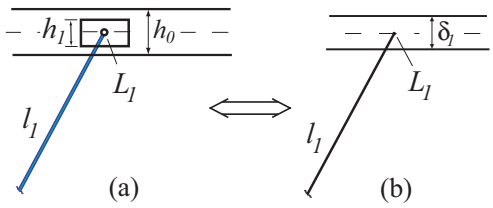

Figure 3: Translational joint with clearance

3 Error workspace analysis of planar four-bar mechanisms

In this section we want to study four-bar mechanisms with joint clearance. The joint clearance of revolute joints are known and described in section 2.1.

3.1 Error workspace of a four-bar mechanism with joint clearance

Now we want to analyze the Pos-EWS and Ori-EWS of an arbitrary end-effector E of a four-bar mechanism. All revolute joints have clearance and the radii of clearance are $\varepsilon_1, \varepsilon_2, \varepsilon_3$ and ε_4. The base points A and B are fixed in the global frame Σ_0. The coupler link (CD) is fixed in the moving frame Σ, see Fig. (4c). Bottema and Roth (1990) have shown the kinematic image of an ideal four-bar motion is the intersection curve d of two hyperboloids $\mathcal{H}_D, \mathcal{H}_C$, see section 1.1. If all joints have clearance, the points D, C in Σ are no longer forced to move on circles (A, l_1) and (B, l_3). They can move on rings defined by $R_D = (A, l_1 \pm (\varepsilon_1 + \varepsilon_2))$ and $R_C = (B, l_2 \pm (\varepsilon_3 + \varepsilon_4))$, see section 2.2. The point D moves in the ring R_D. The kinematic mapping $\varkappa$ maps the corresponding (restricted) three-parametric motion of D to points of a solid $\mathcal{H}_{R_D}$. The boundary of $\mathcal{H}_{R_D}$ consists of two (quasielliptically) coaxial versions of the hyperboloid $\mathcal{H}_D$ (they belong to the radii $l_1 \pm (\varepsilon_1 + \varepsilon_2)$). They will be called $\mathcal{H}_D^+$ and $\mathcal{H}_D^-$. For the point C we have the same situation: The boundaries of the corresponding solid $\mathcal{H}_{R_C}$ are coaxial hyperboloids $\mathcal{H}_C^+$ and $\mathcal{H}_C^-$, see Fig. (4a). The kinematic image of the possible displacements of the end-effector of the four-bar-linkage (due to our restrictions) is therefore the intersection of the two solids $\mathcal{H}_{R_D} \cap \mathcal{H}_{R_C}$. This solid is a certain "pipe" with spine curve $\mathcal{H}_D \cap \mathcal{H}_C$ bounded by the four surfaces $\mathcal{H}_C^+, \mathcal{H}_C^-$ and $\mathcal{H}_D^+, \mathcal{H}_D^-$ (Fig. (4b)).

The possible positions of an end-effector $E \in \Sigma$ define the end-effector workspace W_E (Pos-EWS) in the fixed frame Σ_0. Taking part 1 into consideration, we have $W_E = \gamma_E(\mathcal{H}_{R_D} \cap \mathcal{H}_{R_C})$. Fig. (4c) displays this region for an example. The red curve is the coupler curve c_E of E, which belongs to the nominal model (without clearance).

Now we will have a look on the shape of the "pipe" $\mathcal{H}_{R_D} \cap \mathcal{H}_{R_C}$. The intersections (slices) with the horizontal planes $X_3 = tan(\frac{\varphi}{2})$ belong to fixed angles φ. So the EWS with respect to a fixed orientation of the point E can be determined, see Fig. (4d). In this way we can describe the Ori-EWS. The planes $X_3 = tan(\frac{\varphi}{2})$ intersect the solids $\mathcal{H}_{R_D}$ and $\mathcal{H}_{R_C}$ into two rings. The map γ_E maps them into two rings in Σ_0. Their intersection defines the Pos-EWS for the point E for the fixed angle φ. In Fig. (4b) we can see some cases of ring-ring intersections which belong to the EWS. To study all cases of ring-ring intersections, it is useful to know the accurate values of the coordinates of X_{3a}, X_{3e} of the ring-ring intersections where X_{3a} starts and X_{3e} ends. With these coordinates X_{3a}, X_{3e} the ring-ring intersections can be classified. To find these coordinates we have to solve the following two problems: The first problem refers to Fig. (5a). The sum of the circle radii $(r_{ax} + r_{bx})$ has to be equal to the distance of the circle centers $d(M_a, M_b)$. The centers M_a and M_b are points of the axis a_A and a_B of the solids $\mathcal{H}_{R_D}$ and $\mathcal{H}_{R_C}$. If the fixed points A and B have the Cartesian coordinates $A(A_X, A_Y)$ and $B(B_X, B_Y)$ in Σ_0 and the points C and D (fixed in Σ) have the coordinates $C(c_x, c_y)$ and $D(d_x, d_y)$ in Σ and by setting for example $r_a = l_1 + (\varepsilon_1 + \varepsilon_2)$ and $r_b = l_2 + (\varepsilon_3 + \varepsilon_4)$, the outer contacts of these two (extreme) hyperboloids of the solids $\mathcal{H}_{R_D}$ and $\mathcal{H}_{R_C}$ can be found by solving the following equation (see section 1.1).

$$\frac{r_a}{2}\sqrt{(1 + X_3^2)} + \frac{r_b}{2}\sqrt{(1 + X_3^2)} = \|\mathbf{M_a M_b}\|. \tag{9}$$

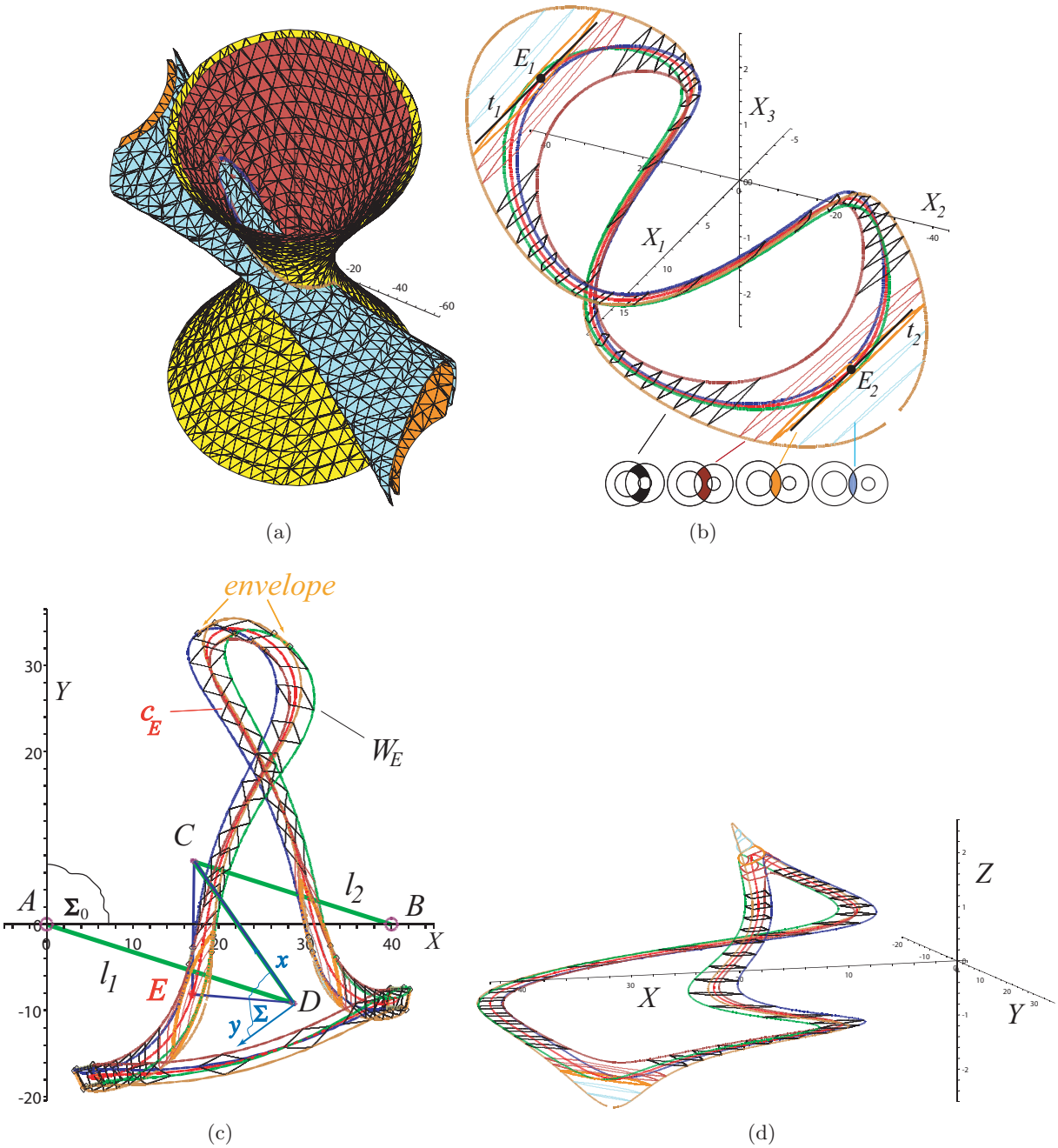

Figure 4: a) and b) Intersection of two solids c) Pos-EWS d) Pos-EWS with orientation

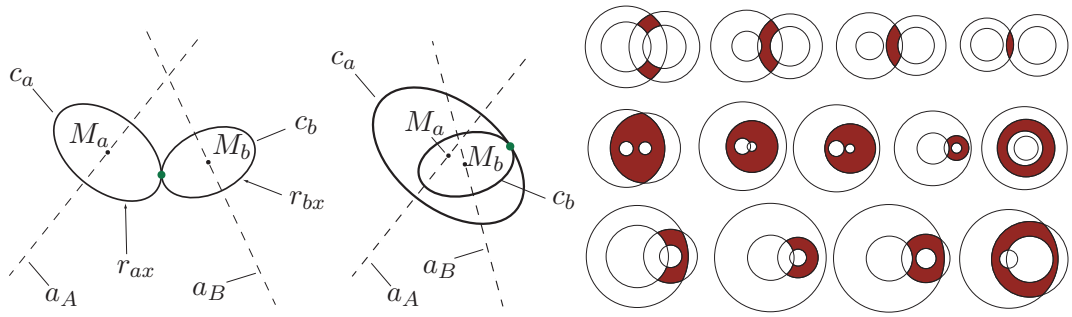

Figure 5: a) and b) outer and inner contact of two hyperboloids c) ring-ring intersections

In a next step we square eq.(9):

$$\left(\frac{r_a}{2}\sqrt{(1+X_3^2)}+\frac{r_b}{2}\sqrt{(1+X_3^2)}\right)^2=\|\mathbf{M_aM_b}\|^2. \tag{10}$$

Evaluation of eq.(10) gives an equation, which is in X_3 an algebraic expression of order two. So the coordinates X_{3a} and X_{3e} for the outer contacts can be determined accurately . The second problem refers to Fig. (5b). The equation of the inner contacts of two hyperboloids is also of order two, equation (11) is of similar difficulty as the first problem.

$$\frac{r_a}{2}\sqrt{(1+X_3^2)}-\frac{r_b}{2}\sqrt{(1+X_3^2)}=\|\mathbf{M_aM_b}\|,\quad \text{if } r_a\geq r_b. \tag{11}$$

With these results it is easy to analyze the EWS for an arbitrary orientation. Furthermore, now it makes sense to define 13 cases of ring-ring intersections, see in Fig. (5c). Note, some cases are only for big clearance possible. In Fig. (4b) we display the four cases of ring-ring intersections which belong to our four-bar mechanism.

Remark 4. If the image curve (see the red curve of Fig. (4b)) of the nominal four-bar motion has points E_1, E_2 with horizontal tangents t_1, t_2, these two points belong to two instantaneous translations. For these orientations leg l_1 and leg l_2 are parallel. And if this nominal mechanism has joint clearance the horizontal planes generally intersect the EWS $\in \mathbb{P}^3$ "close" to the points E_1 and E_2 in local large areas (see the orange Pos-EWS in Fig(4)).

In order to describe the boundary of the Pos-EWS we use the definition of contour and silhouette of a surface Φ with respect to a γ_E-image.

Definition 1. The contour $c(\Phi)$ of a surface Φ with respect to the projection γ_E is the set of all points $X \in \Phi$ which tangent planes at X contain lines of the congruence LC_E. The image $\gamma_E(c(\Phi))$ is the silhouette $s(\Phi)$ of Φ with respect to γ_E.

As stated before, the EWS of a point $E \in \Sigma$ is given by $W_E = \gamma_E(\mathcal{H}_{R_D} \cap \mathcal{H}_{R_C})$. The boundary of this region consists of same parts: They either belong to the γ_E- images of the four intersecting curves of the boundary surfaces $\mathcal{H}_D^+, \mathcal{H}_D^-$ with $\mathcal{H}_C^+$ and $\mathcal{H}_C^-$ or are parts of the silhouettes (with respect to γ_E) of these four surfaces.

Remark 5. The surface Φ is a called Clifford-cylinder. There exist two one-parametric groups of quasielliptic translations which keep Φ invariant. Its point paths on Φ are the two series of generators. One of these groups of translations keeps the net γ_E invariant. Therefore the contour of Φ with respect to γ_E has to consist of such generators. As the silhouette of Φ consists of two concentric circles. For example for $\mathcal{H}_D^+$ the two circles have the radii $rs_o = \|\mathbf{DE}\| + r_a$ and $rs_i = \|\mathbf{DE}\| - r_a$. The real part of the contour (as its preimage) splits into two generators on Φ.

The boundary of the EWS of a point E consists of parts of the γ_E-images of the four intersecting curves of $\mathcal{H}_D^+, \mathcal{H}_D^-$ with $\mathcal{H}_C^+$ and $\mathcal{H}_C^-$ and some parts of circles, which are gained as silhouettes of the surfaces $\mathcal{H}_C^+, \mathcal{H}_C^-, \mathcal{H}_D^+, \mathcal{H}_D^-$. The intersection points of the generators and the EWS can also be found accurately because these points are the intersection points of a line and of an hyperboloid. So we can determine the boundary of the Pos-EWS analytically. The determination of the EWS also works, if the joint clearance increases.

3.2 Error workspace of replacement mechanisms

In this subsection we want to look at the Pos-EWS of the two replacement mechanisms for the given four-bar mechanism (A, B, C, D) in Fig. (4). Fig. (6a) shows all three mechanisms which describe the same coupler curve c for the end-effector E (their orientations are different). But what happens if all joints have the same radii of clearance? The results are shown in Fig. (6b) and Fig. (6c). All three nominal mechanisms describe the same coupler curve c, but we can see

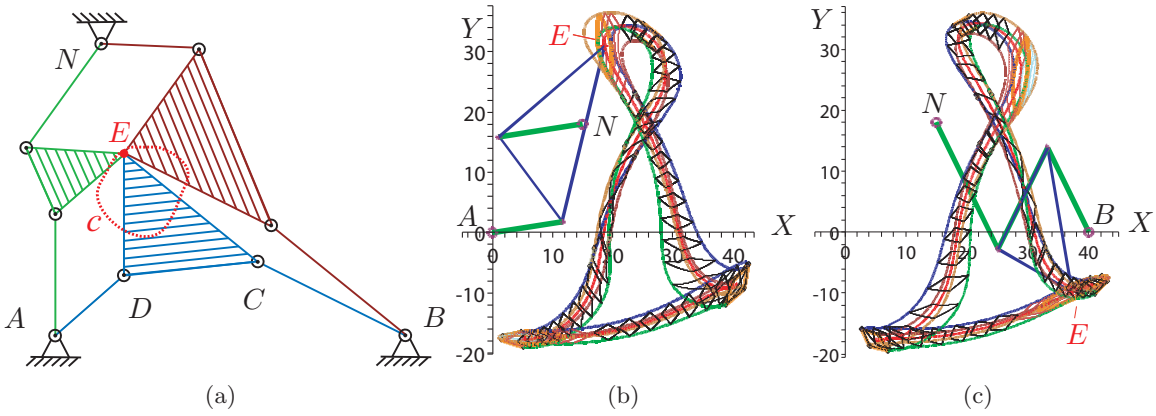

Figure 6: Pos-Error workspaces of replacement mechanisms

the Pos-EWSs are different. The part of the interest on the coupler curve could influence the choice of a qualified replacement mechanism.

3.3 Folding four-bar mechanism

The coupler curve c of an end-effector E can have two different branches which are strictly separated, see Fig. (7a). Due to the joint clearance, it could be possible that these separated branches can be reached without destroying the mechanism see Fig. (7c). These mechanisms are folding mechanisms due to joint clearance. For such a mechanism it is interesting to find the

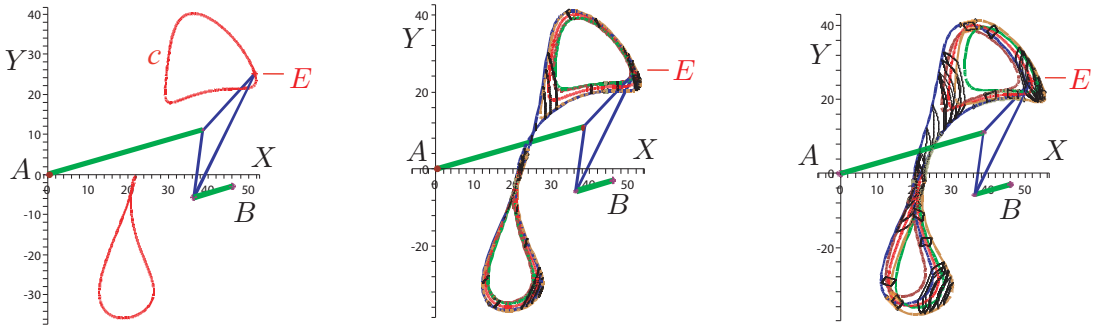

(a) (b) (c)

Figure 7: Pos-Error workspaces of an folding four-bar mechanism

value of clearance so that the mechanism becomes a folding mechanism: We add clearance to the leg lengths and apply the conditions for "folding four-bars", see Wunderlich (1968) and Bottema and Roth (1990). In our concept these belong to the double solution of the inner contact of eq.(11) of the hyperboloids $\mathcal{H}_C^+, \mathcal{H}_D^-$ or of the hyperboloids $\mathcal{H}_D^+, \mathcal{H}_C^-$. One case is worked out here. Fig. (7) shows an example – (7a) displays the situation without clearance. Then the clearance increases. Part (7b) shows a "folding case" situation, which is crossed in part (7c).

4 Error workspace of multi loop mechanisms

In this section we want to study the EWS of two multi loop mechanisms with revolute joints.

4.1 Double-rocker four-bar mechanism

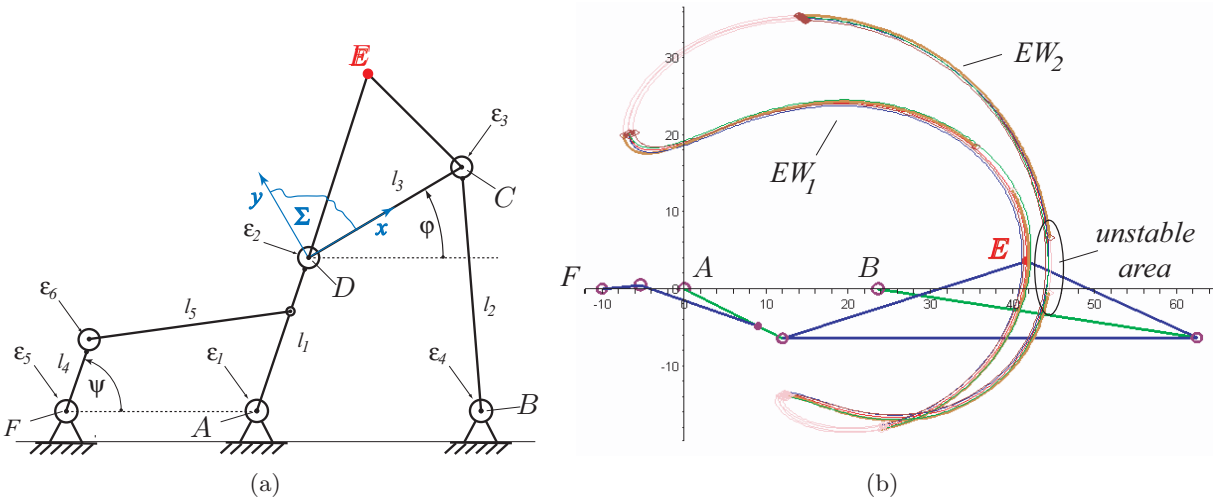

(a) (b)

Figure 8: Pos-Error workspace of a Double-rocker four-bar mechanism with driving crank

Fig. (8a) shows a four-bar mechanism $ABCD$ with driving crank link l_4. This mechanism has two closed loops. In a first step we want to analyze the EWS of E when the mechanism has joint clearance with radii $\varepsilon_1, \varepsilon_2, \varepsilon_3, \varepsilon_4, \varepsilon_5$ and ε_6, see Fig. (8a). We can see in Fig. (8b) the whole Pos-EWS of the four-bar mechanism (A, B, C, D, E) which is separated into two areas EW_1 and EW_2 due to the driving crank l_4. We can see some disconnected curves in EW_1 and EW_2. One of them is the red coupler curve of the nominal mechanism in EW_2. If the nominal end-effector E is designed to follow the path in EW_2, the mechanism will have a folding position due to joint clearance. The boundary of the EWS EW_1 and EW_2 can be found analytically.

4.2 Film pull-down mechanism

Fig. (9) shows a film pull-down mechanism with joint clearance. The end-effector E is designed to follow the red path c. Now we want to study the unconstrained motion of the moving frame $\Sigma = [H, F, E]$ by taking into account joint clearance with radii $\varepsilon_1, \varepsilon_2, \varepsilon_3, \varepsilon_4, \varepsilon_5$ and ε_6. The unconstrained motion of Σ could be described as follows: The origin O of Σ has to move on the Pos-EWS of the four-bar mechanism (A, B, C, D) with end-effector H and the point F (fixed in Σ) has to follow a ring with center G (fixed in Σ_0).

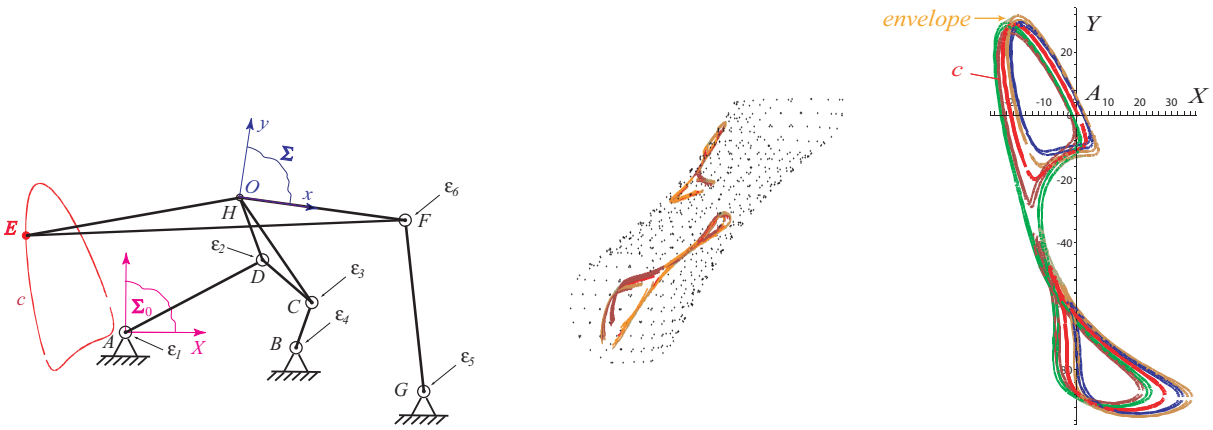

(a) (b) (c)

Figure 9: Error workspace of a film pull-down mechanism

Now we study the motion of our new frame Σ: The Pos-EWS of H with respect to the four-bar motion has a boundary b_0. If O (now fixed in Σ) moves on this boundary b_0, the kinematic image of this motion is a ruled surface. Their generators are described in remark (1) or in remark (2). So we have a parametrization of this ruled surface. Because of joint clearance the point F moves on a ring. The corresponding kinematic image is a solid bounded by two hyperboloids of rotation. The kinematic image of the motion of the frame Σ is the intersection of these two solids. The boundary of this intersection, see Fig. (9b) can be given in parametric form because one of the solid is bound by two coaxial hyperboloids. The EWS can be separated into several parts, see Fig. (9b). The film pull-down in Fig. (9a) has a folding position due to joint clearance. In Fig. (9c) we can see the connection of two paths of the end-effector E although the end-effector E is designed only to follow one path c, see Fig. (9a). Due to the design of this mechanism, only one part of the EWS in the image space is interesting. The mapping γ_E of

this EWS is the Pos-EWS of E. This Pos-EWS is bound by the mapping γ_E of the intersection curves and of the corresponding silhouettes. Some parts of these silhouettes can only be found numerically.

5 Error workspace of a slider-crank mechanism

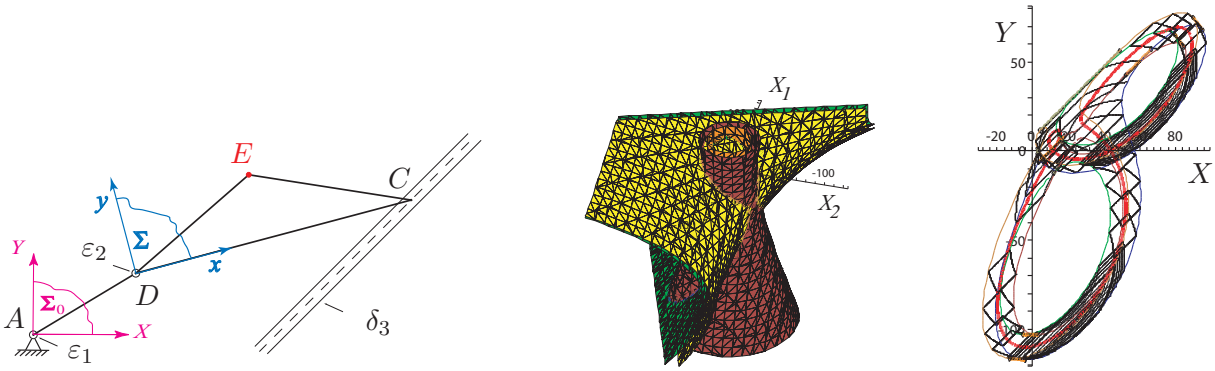

(a) (b) (c)

Figure 10: Error workspace of a slider-crank mechanism

Similar as in section (3.1) we get the EWS of a slider-crank mechanism. Fig. (10) shows a slider-crank mechanism with joint clearance. The revolute joints have the radii of clearance ε_1 and ε_2 and the transmission joint has a strip of clearance δ_3. The coupler link (CD) is fixed in the moving frame Σ. The kinematic image of Σ that D moves on the ring R_D and C moves on a strip is the intersection of two solids which are bound by two coaxial hyperboloids and two hyperbolic paraboloids. The silhouette of an hyperbolic paraboloid consists of two lines. They are parallel to the translational axis. The contour of an hyperbolic paraboloid consists of two generators meeting the absolute line u, see remark (5). Parallel planes $(X_3 = const)$ intersect the solids in one ring and in one strip. We can define some classes of ring-strip intersections and similar as in section(3.1), we can accurately determine the contact points. The Pos-EWS of the end-effector E in Fig. (10c) is determined analytically. The red curve in Fig. (10c) is the path of E if the mechanism is ideal.

6 Conclusion

Assuming perfect joint clearance we showed that the Error Error workspace of some planar mechanisms can be described analytically. For studying the Error workspace the kinematic image space was used. We classified the EWS of a four-bar mechanism and of a slider-crank mechanism. We compared the Pos-EWS of a four-bar mechanism with its replacement mechanisms and studied folding four-bar mechanisms due to joint clearance. Then we extended the considerations to further planar mechanisms. The determination of the EWS also works, if the joint clearance increases.

References

R. Bereis. Über das Raumbild eines ebenen Zwanglaufes (kinematische Abbildung von Blaschke und Grünwald). *Wissenschaftliche Zeitschrift der Technischen Universitt Dresden*, 13(1):7–16, 1964.

W. Blaschke. Kinematik und Quaternionen. *VEB Deutscher Verlag der Wissenschaften*, 1960.

O. Bottema and B. Roth. *Theoretical Kinematics*. Dover Publications, 1990.

K. Frick. Kinematic tolerance analysis of planar mechanical systems. *Master Thesis*, 2004.

C. Hörsken. Methoden zur rechnergestützen Toleranzanalyse in Computer Aided Design und Mehrkörpersystem. *Dissertation, rel. in Fortschritt Berichte VDI Reihe*, 20, 2003.

M. Husty. On the workspace of planar three-legged platforms. In *ISRAM-World Congress of Automation*, volume 3, pages 1790–1796, 1996.

F. Pernkopf and M. Husty. Reachable workspace and manufacturing erros of stewart-gough manipulators. In *Proceedings of MUSME*, Uberlandia, Brazil, 2005.

H.-P. Schröcker and J. Wallner. Curvatures and tolerances in the euclidean motion group. *Results Math.*, 47:132–146, 2005.

H. Stachel. Zur quasielliptischen Differentialgeometrie. *Berichte der Math.-Stat. Sektion im Forschungszentrum*, 80:1–38, 1970.

M. Tsai and T. Lai. Kinematic sensitivity analysis of linkage with joint clearance based on transmission quality. *Mech. Mach. Theorey*, 39:1189–1206, 2004.

P. Voglewede and E. Uphoff. Application of workspace generation techniques to determine the unconstrained motion of parallel manipulators. *ASME Journal of Mechanical Design*, 126: 283–290, 2004.

J. Wallner, H.-P. Schröcker, and S. Hu. Tolerances in geometric constraint problems. *Reliab. Comput.*, 11:235–251, 2005.

J. Wittwer, W. Kenneth, and L. Larry. The direct linearization method applied to position error in kinematic linkage. *Mech. Mach. Theorey*, 39:681–693, 2004.

K. Wohlhart. Degrees of shakiness. *Mech. Mach. Theorey*, 34:1103–1126, 1999.

W. Wunderlich. *Ebene Kinematik*. Hochschultaschenbücher-Verlag, 1968.